A SYNTHETIC SENSOR/IMAGE SIMULATION TOOL TO SUPPORT THE LANDSAT DATA CONTINUITY MISSION (LDCM)

John R. Schott, Professor
Rolando V. Raqueno, Scientist
Nina G. Raqueno, Scientist
Scott D. Brown, Scientist
Digital Imaging and Remote Sensing Laboratory
Chester F. Carlson Center for Imaging Science
Rochester Institute of Technology
Rochester, NY 14623
schott@cis.rit.edu
rolando@cis.rit.edu
nina@cis.rit.edu
brown@cis.rit.edu

ABSTRACT

The next generation of Landsat sensors will incorporate many changes from the existing whiskbroom designs. In particular, the Operational Land Imager (OLI) incorporates a multispectral pushbroom design which has different bands imaging the same spot on the Earth at slightly different angles and times. This requires more involved knowledge of the sensor and the scene, as input to more complex processing algorithms, to form spectrally registered images. In addition, the thermal data for the LDCM will come from a separate Thermal Infrared Sensing Instrument (TIRS) flown on the same platform. Thus, there are additional complexities associated with registering the OLI and TIRS data to each other and the ground. This paper presents a synthetic sensor/scene model designed to generate synthetic OLI and TIRS data sets to support development and testing of LDCM image reconstruction algorithms. This is part of a larger effort to use the synthetic sensor/scene models to support a range of LDCM development and monitoring activities. Methods for generation of a synthetic scene incorporating digital elevation models, spatial texture from high resolution satellite data, spectral variability from Hyperion satellite data, and atmospheric effects from the MODTRAN radiative transfer code are presented. Within the Digital Imaging and Remote Sensing Image Generation model, OLI and TIRS sensor models are being created that can be "flown" over the synthetic scene to form synthetic images that mimic the geometric sampling of the actual sensors. The synthetic images will be used to support the Landsat image quality assessment program with an initial focus on image reconstruction algorithms

INTRODUCTION

The Landsat Data Continuity Mission (LDCM) is the next stage of the Landsat series of medium resolution, Earth observing orbital sensors. The LDCM will carry two new instruments. The Orbital Land Imager (OLI) will have eight 30 meter multispectral bands and a 15m panchromatic sharpening band. The Thermal Infrared Sensor (TIRS) will have two 100 meter multispectral bands (see Irons and Murphy-Morris 2007). To form the final image products from LDCM, the data from the two instruments will be terrain corrected, geospatially registered and the 100m thermal bands resampled to 30m to produce an 11 band image product. This fusion of data from two instruments represents a new paradigm for Landsat. In addition, both instruments use pushbroom array technology which is also new to Landsat. This new approach should provide more spectral coverage and better signal-to-noise than the current Landsat ETM+ data (see Markham et al. 2008). However, this new design also presents a number of new challenges that must be incorporated into the Landsat data production process. The new pushbroom geometry means the band-to-band spectral registration, inherent in the traditional Landsat whiskbroom scanners, must be approximated using fully terrain corrected resampling techniques. This band-to-band registration issue is even more difficult when registering the thermal bands since they are acquired by a different sensor. The radiometric calibration of the new instruments is complicated by a dramatic increase in the number of individual detector elements (from less than 200 to over 100,000) all of which need to be cross calibrated (detector-to-detector) to each other. The wider field of view telescopes on the new instruments coupled with the use of multiple detector arrays

and filter sets complicates the absolute and spectral calibration. These, plus a host of other issues must be dealt with in achieving and maintaining the long term image quality needed to support the Landsat program.

Simulation and modeling tools represent one way to support a number of the design, implementation and operational studies expected to arise over the lifetime of the LDCM. The overall image quality is a function of the complex interplay of the scene, illumination, atmosphere, sensor location and orientation, and sensor characteristics. Thus, a model suitable for predicting and evaluating image quality must incorporate all the relevant scene, acquisition, and sensor phenomenology. To this end, NASA, through the Rochester Institute of Technology (RIT), has initiated a program to build a synthetic scene-senor model to support the LDCM. This modeling tool built using RIT's Digital Imaging and Remote Sensing Image Generation (DIRSIG) model is designed to produce end-to-end image simulations incorporating all the relevant characteristics of LDCM images. This is a multiyear effort with a spiral development approach. This paper addresses the first year's efforts which, include baseline OLI and TIRS sensor models and an initial synthetic scene of a $364\,\mathrm{km}^2$ region encompassing part of Lake Tahoe. The first spiral has emphasized image geometry issues and the OLI sensor. The TIRS sensor and related geometry issues have also been initialized though only limited effort has been spent to date on the thermal aspects of the synthetic scene. This paper presents the sensor (Section 2), scene (Section 3) and image formation (Section 4) modeling approach and the initial image products (Section 5).

SENSOR AND PLATFORM SIMULATION

This section describes how the OLI and TIRS sensors and orbital platform models are being implemented in DIRSIG. Most of the implementation takes advantage of existing DIRSIG capabilities (see Schott et al. 1999 and Schott 2007). However, several new capabilities have been added to DIRSIG to support the LDCM model.

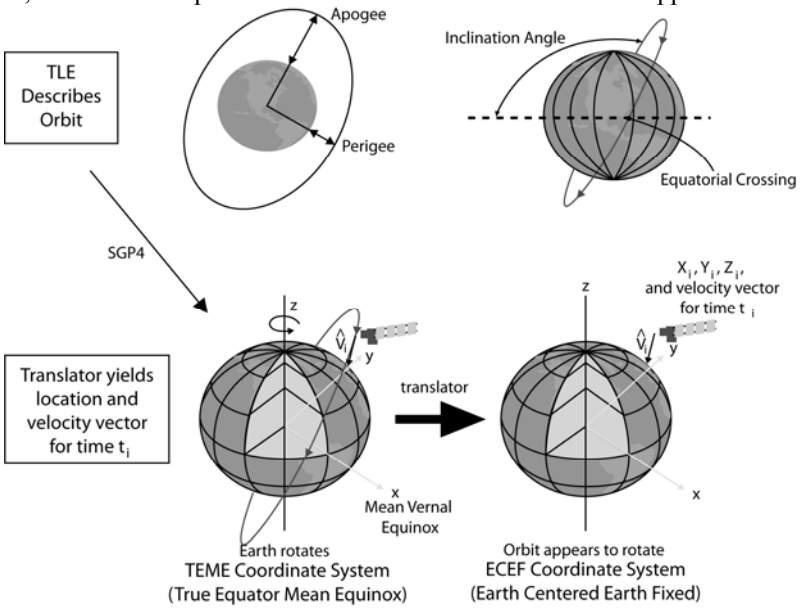

Figure 1. Conceptual representation for how the Two Line Element (TLE) orbital descriptors are used to generate DIRSIG ECEF coordinates and velocity vectors.

Orbital Path and Reference Coordinate System

As part of recent upgrades, DIRSIG now provides for orbital descriptions using the standard North American Aerospace Defense Command (NORAD) Two Line Element (TLE) orbital descriptors. Regularly updated TLE descriptors are available for most spacecraft. The TLE descriptors are a compact means of describing the detailed orbital path of a spacecraft. In the DIRSIG implementation, they are translated into an orbital location and velocity vector using Simplified General Perturbations Version 4 (SGP4) (cf. Vallado and Crawford 2008). The output is in a True Equator Mean Equinox (TEME) coordinate system which must be further translated into the Earth Centered-Earth Fixed (ECEF) format which DIRSIG uses (see Figure 1). This results in an X, Y, Z location and velocity vector, for each sample time, in the ECEF data format. Conveniently, the inverse of the location vector (-X,-Y,-Z) is

the nominal pointing vector for the imaging sensors. The satellite location is recalculated for each clock cycle desired (e.g. sample time), yielding a detailed satellite track and nominal pointing angle.

Platform: Sensor Location, Pointing and Jitter

The DIRSIG sensor model recognizes that the sensors on a space platform are not typically located at the satellite's center of mass as reported by the TLE. Furthermore, the spacecraft orientation and the optical axis of each instrument may have both structured and random (jitter) pointing deviations from the nominal Line of Sight (LoS) to the center of the Earth. These location and pointing characteristics can all be programmed into DIRSIG as shown in Figure 2. Note that, in general, low frequency or structured pointing data are used to change the LoS of each instrument and high frequency variation is used in aggregate to introduce blur through the sensor Modulation Transfer Function (MTF) (see Section 2.5). The location and pointing knowledge of each sensor relative to the platform, coupled with the overall satellite location and pointing provide the sensor's external geometry (i.e., location and orientation) as shown in Figure 2.

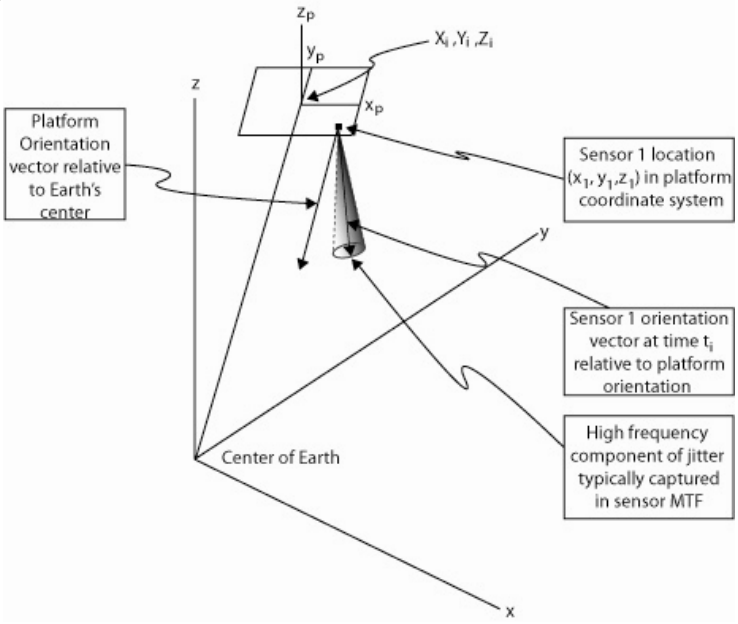

Figure 2. Conceptual illustration of the DIRSIG platform instrument and pointing model showing a platform with a single sensor. The user supplies pointing knowledge for the platform and each sensor as a function of time.

Camera Model: Focal Plane Layout

The DIRSIG camera model allows the user to input a focal length and to arrange individual detectors or detector arrays on the focal plane to build the internal camera geometry as shown in Figure 3a. For conceptual designs this approach is simple to implement and often sufficient. However, for the OLI and TIRS instruments, we have more detailed knowledge in the form of angular location of each individual detector element (see Figure 3b). Note that, because the angle-angle descriptors are observed data from the instrument test chamber, they incorporate all the optical distortions of the actual flight instrument. A Look Up Table (LUT) is used to relate the detector element sampling sequence to the angle-angle location of the detectors (see Figure 3c) allowing the user to update how the sensor is operated in the simulation. Both of these sensor description models provide the internal camera geometry allowing DIRSIG to trace rays from the detector through the focal point into the scene (see Section 4). Note that in Figure 3 and throughout this paper we have projected the image plane through focus onto a plane one focal length below the focal point. This is a common convention in photogrametry and is regularly used in the DIRSIG literature. Each pixel in a row for each array is sampled (or oversampled-see Section 2.6) at a clock pulse (i.e., at a satellite location). The image is formed (as with the actual instruments) by the forward motion of the spacecraft and sequential samples. The resulting data stream must be resampled in the same manner as the actual data to form rectilinear, spectrally registered images of the ground.

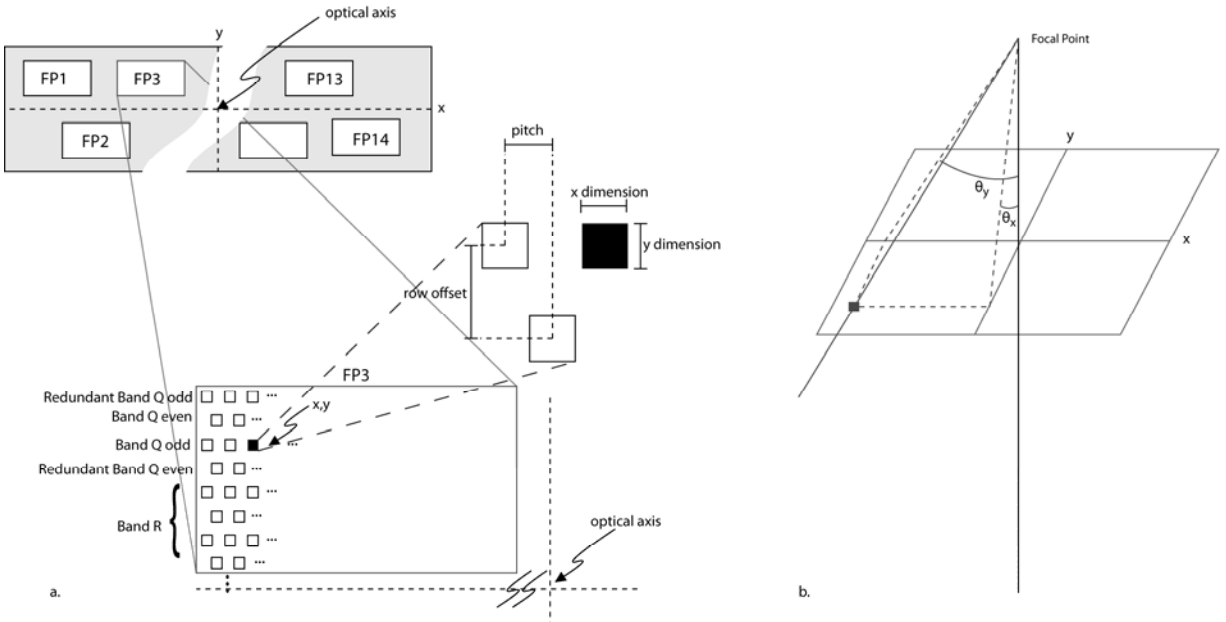

Sequential Detector Sample Locations

Focal Plane Module	Band	Primary/ Redundant	Odd/Even	Detector
1	1	Primary	Odd	1
1	1	Redundant	Even	1
1	1	Primary	Odd	2

Look Up Table

Designator	θ_x	θ_y
11P01	0.0071	0.0072
11RE1	0.0076	0.0076
11P02	0.0072	0.0074

c.

Figure 3. a; Internal camera geometry using focal plane spatial locations, b; Internal camera geometry using angular location representations for each detector element and c; Use of a LUT to map from geometric read sequence to angle-angle sample locations.

Relative Spectral Response (RSR)

The DIRSIG tool allows the assignment of a relative spectral response (RSR) to be assigned for each band at various levels (conceivably down to the individual detector element). For the first spiral, RSR values will be assigned for each spectral band at the focal plane array level, as this is consistent with our current knowledge levels. As the knowledge levels grow, different RSR values can be assigned to different lines of data within an array, if appropriate, or to individual detector elements in later spirals.

TIRS Implementation

The emphasis of this paper is on the OLI instrument which is the focus of the first development spiral. However, the DIRSIG model of the TIRS instrument is following a parallel development with a short lag. The TIRS instrument model will be located on the same simulated vehicle but with an offset that mimics the actual TIRS instrument offset. The TIRS optical axis and pointing variation can all be controlled independently of OLI. However, as with the actual instruments, the TIRS and OLI instruments can share a common clock to control instrument sampling. The TIRS pushbroom focal plane will be modeled in essentially the same way as the OLI instrument with detector location knowledge expressed in an angle-angle format relative to the optical axis. Rays traced through the center of the pixel and at angles about the center that are enclosed in the Point Spread Function (PSF) of the instrument provide for sampling the scene radiometry (see Section 4) on a pixel by pixel basis for either instrument.

Spiral Development

To facilitate use for various design, testing, monitoring and scientific applications, the DIRSIG models are being developed using a spiral development approach. This allows for the early release of a basic capability (which is the focus of this paper) followed by successive releases with increasing capabilities and greater fidelity to the actual data stream expected from LDCM. The priority for the first spiral has been to establish the basic capability for a small scene with an emphasis on capturing the core geometric sampling characteristics of the instruments. Priorities for future spirals will be dictated in part by program priorities. Some of the developments currently planned for the second spiral (4^{th} quarter 2010) include detector noise, detector timing and readout sequencing designed to mimic actual data sequences (i.e., arrays readout in the same pattern as actual data) and detector area sampling using initial instrument PSFs (note the first spiral allows for oversampling but assumes a simple sampling function (e.g., rectangular) see Figure 4).

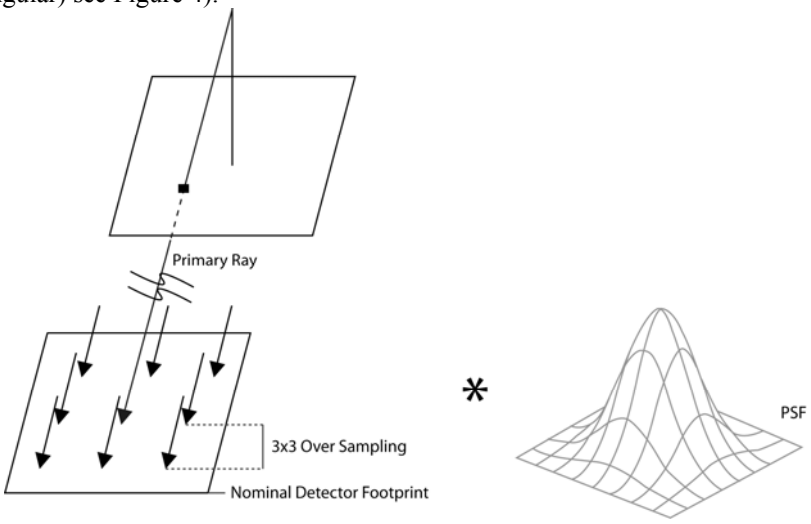

Figure 4. Illustration of the sampling of a single pixel showing 3x3 over sampling with angular sample spacing $\Delta\theta_x$, $\Delta\theta_y$. The over sampled data is then convolved with the PSF for each band or array within a band.

Scene Generation

DIRSIG scenes have traditionally been relatively small and designed for imaging at high resolution (i.e., fractions of a meter to a few meters). For initial testing of the geometric, radiometric and cross registration characteristics of the LDCM sensors a larger scene was required but not necessarily the full 185 km swath of LDCM, since any portion of the sensor could be "flown" over the scene to test phenomena of interest. For practical purposes, a 13 km wide region, including the southwest corner of Lake Tahoe, was chosen for the target scene in spiral 1. The site was chosen for its high topographic relief (over 1 km), the availability of high resolution satellite data, EO-1 Hyperion data and a significant amount of day and night Landsat data.

Surface Geometry

DIRSIG uses an East-North-Up (ENU), X,Y,Z rectilinear coordinate system whose origin is tied to a user defined point on the Earth. The Earth's surface and objects in the scene are described by facetized surfaces. To form a Landsat scene a digital elevation model (DEM) referenced to the WGS 84 Geoid is used to form an angle-angle-distance polar representation of every post in the DEM using the latitude-longitude and height information in the DEM (see Figure 5). The points in polar coordinates are then translated to the DIRSIG native ENU coordinate system which is tied to a point in the scene (see Figure 5). The posts are then facetized into a Triangular Irregular Network (TIN) using standard graphics TINing software.

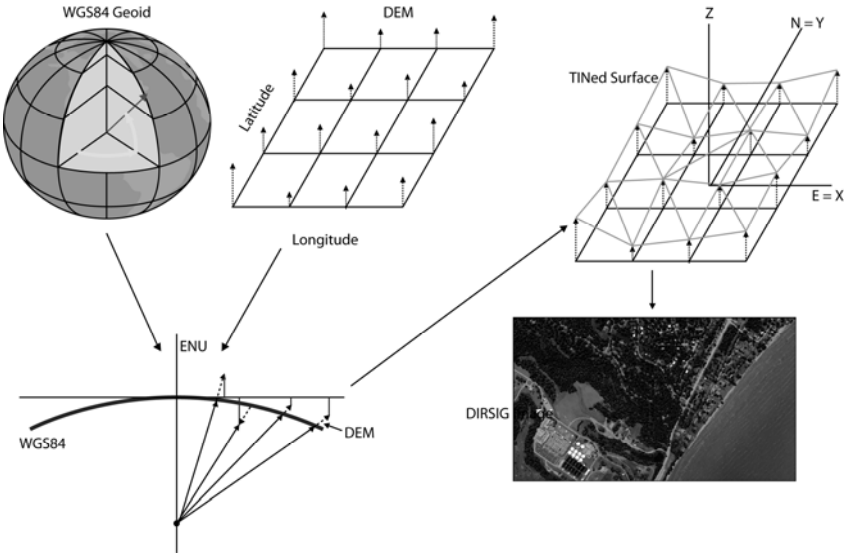

Figure 5. Illustration of how a WGS84 Geoid and a DEM are translated from polar latitude-longitude-distance to DIRSIG's native East-North-Up (ENU) rectilinear coordinate system. The data are then TINed, and facetized objects are added which can be rendered in a final DIRSIG image.

Object Geometry

DIRSIG uses a facetized representation of objects such as trees and buildings located on the terrain. For the first spiral no objects will be placed in the scene. However, trees and buildings may be explicitly added in later spirals to allow more complex modeling of bidirectional reflectance distribution function (BRDF) effects to support understanding of radiometric issues affecting atmospheric compensation and mosaic generation (see Figure 6).

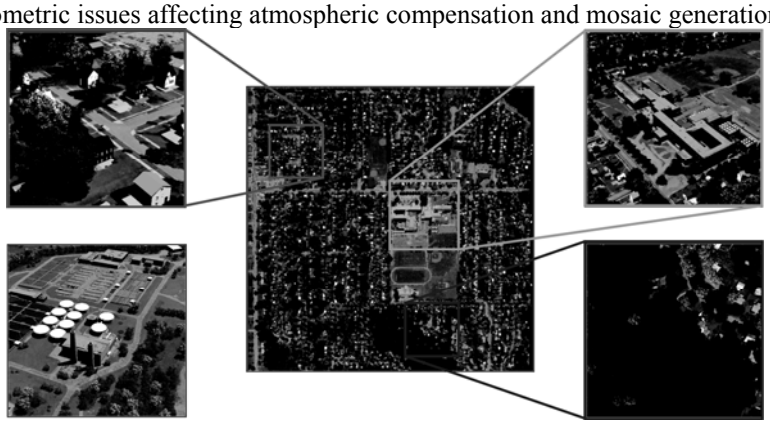

Figure 6. DIRSIG true color scene of a residential neighborhood. Note the individual trees contain thousands of facets and the tonal variations are caused by spectral reflectance, spectral transmission, crown density, and overall crown structure.

Object Attribution

Each surface in a DIRSIG scene has optical and thermodynamic attributes assigned to it at the facet or subfacet level. The optical properties include bidirectional reflectance distribution functions (BRDFs) and where appropriate, optical transmission as a function of wavelength across all relevant spectral ranges. The thermodynamic properties include solar absorption and thermal emissivity which are calculated from the optical properties by weighting by the solar illumination spectrum and the blackbody emission spectrum, respectively. In addition, the thermal conductivity, specific heat, density, and thickness of the materials are needed to drive DIRSIG's thermodynamic model. Other parameters such as solar illumination history, slope, aspect and exposed sky fraction are collected at run time by the DIRSIG ray tracer (see Section 4.1). Material attributes can be assigned when objects are created or by projection onto a surface using texturing tools (see Scanlan et al. 2003).

To build the first LDCM scene the following data were registered to the DEM of the site (~ 10 m posts): Digital Globe 4 band image acquired 06/28/2004 (13 km x 28 km) which defines the extent of the initial scene, EO-1-

Hyperion Image acquired 08/30/2004, and an ASTER emissivity map (Hulley et al. 2008) (see Figure 7). The high resolution (~4 m) data were classified using an unsupervised classifier into 9 classes. These classes were assigned names by photo interpretation of the high resolution, Landsat and Hyperion imagery and the DEM. The classes are also assigned initial bulk properties (specific heat, etc) needed to run the thermal model based on existing DIRSIG database values for similar materials. This class map was then used to train a supervised classifier which was applied to the overlapping region of the Hyperion image. For each class, the radiance/reflectance spectra associated with the Hyperion pixels are then used to form a spectral library for each class. Because an Empirical Line Method (ELM) atmospheric compensation has been applied to these data, the spectral libraries are available either as radiance spectra or reflectance spectra. Note future spirals will use Hyperion data corrected to reflectance on a pixel by pixel basis (see Sanders et al. 2001) to reduce residual elevation induced artifacts in the ELM generated spectra (note that because these artifacts only occur near strong atmospheric absorption features, which the LDCM bands avoid, there should be limited impact on the initial data).

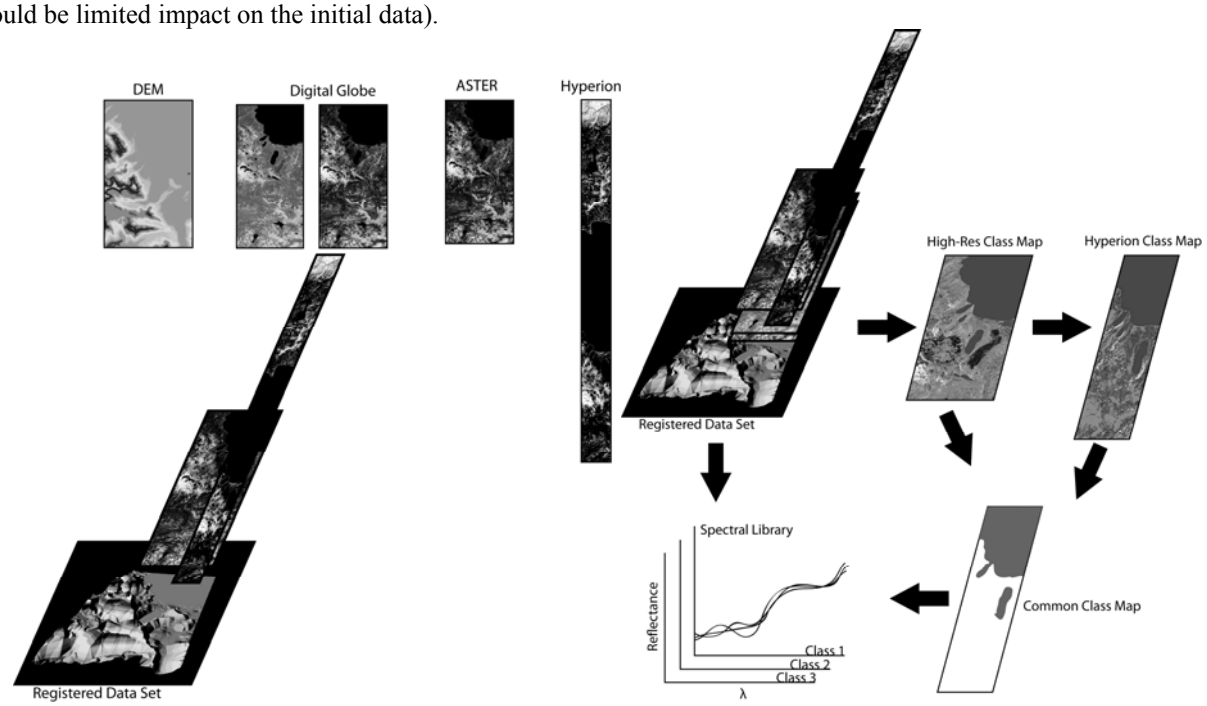

Figure 7. Data used in scene construction. All data are registered to the DEM. The classified high-resolution data are used to classify the Hyperion data and pixels with common classification are used to build spectral libraries representing the range of spectral reflectance for that class.

The DEM, along with the registered high resolution image, high resolution class map, and ASTER emissivity map, are then translated into the native DIRSIG geometry and TINed to form the geometry for the scene. The high resolution image and the emissivity images are now treated as DIRSIG texture maps and are used in conjunction with the class maps to provide most attributes of the scene. The spectral reflectance of each surface for each class is found using the z-score normalized brightness in each of the four high resolution bands (i.e., the brightness is redefined by its signed distance in standard deviations from the mean). The spectral reflectance curve for that location is found by assigning the curve in the Hyperion derived spectral reflectance library that most closely matches the z-score values. The matching takes place on z-score values for the corresponding spectral bands produced from the spectral library data (see Figure 7). For the first spiral the reflectivities are assumed Lambertian. In future spirals, the shape of the BRDFs may be assigned using MODIS BRDF maps while continuing to use the high resolution texture maps to provide the magnitude of the spectral reflectance. The emissivity values are assigned by spectral interpolation from the ASTER maps. The thermal bulk properties will be assigned by class type for the first spiral, with more advanced techniques considered for the later spirals (cf. Ward et al. 2008). The remainder of the data needed to model radiance and temperature can be acquired by the DIRSIG ray tracer as described in the next section. Note that, at this stage, the optical properties are essentially "glued" to the terrain. Future spirals may include planted forests, buildings, etc which is commonly done for higher spatial resolution DIRSIG scenes.

DIRSIG Radiometry and Ray Tracing

The DIRSIG radiometry is extensively treated elsewhere (Schott et al. 1992, Schott et al. 1999 and Schott 2007) and only a brief treatment will be included here since the LDCM modeling uses mostly existing radiometry capabilities.

Ray Tracer

The DIRSIG ray tracer can be thought of as a tool to gather data about the scene. Mathematically, each ray is sampling the scene with a delta function. Conceptually, when a detector element is sampled, a ray is cast from the center of the pixel through the focal point and into the scene. For the LDCM model we will use the common photogrametry convention of projecting the focal plane through focus onto a mirror image of itself a focal length below the focal point. From this perspective the detector elements angular location represents the angle into which the ray is cast from the focal point through the detector element into the scene (see Figure 3). The ray proceeds until it hits an opaque object, gathering information about any transmissive objects it hits along the way (e.g. tree leaves, clouds, atmospheric inhomogeneities…). At the primary hit point (and any preliminary or secondary hit points) the ray tracer gathers information on the location (X,Y,Z), orientation, material class, optical properties (using the texture maps as described in Section 3.3) and thermodynamic properties of the surface it intersects and then sends out a number of secondary rays to gather additional information about the surround (see Figure 8). This includes up to 24 hours of sun shadow history, current solar illumination conditions, as well as, a sampling of the hemisphere above the target so that radiance levels from the sky and surround can be calculated. At each secondary hit point all the same data as at a primary hit point can be gathered. In general, the process is terminated after two and one half hits (i.e., the primary, secondary and solar illumination level on the secondary) but the number of hits is user controlled. The sun-shadow history data are used with a 24 hour weather history file and the thermal data gathered by the ray tracer as input to DIRSIG's thermal model to calculate the temperature of the target (and background hit points if required). Secondary rays that "hit" the sky record the angular location in the sky and return the spectral radiance from that region of the sky as predicted by MODTRAN (see Section 4.2). Secondary rays that hit background objects gather information about the background object and its surround (i.e., temperature, reflectivity, solar illumination level) that is used in the radiometry model to calculate the radiance from that particular background direction. Essentially all the data gathered by the ray tracer and the thermal model are passed to the radiometry model.

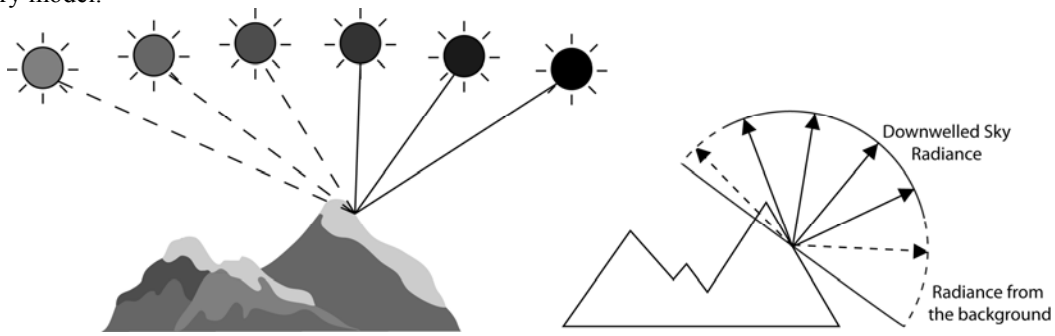

Figure 8. Illustration of how the ray tracer is used to gather information for radiometry calculations including sun shadow history, sky fraction absorbed, and sources of radiance from the surround.

Radiometry Model

For the sake of brevity, we will express the DIRSIG radiometry model using a simplified governing equation that neglects DIRSIG's treatment of transmissive objects along any ray traced path and simplifies DIRSIG's treatment of background radiance sources. The effective in band spectral radiance $\left(L_B\right)$ in band B for a primary ray cast in the $\left(\theta_x, \theta_y\right)$ directions can be expressed as:

$$L_B\left(\theta_x,\theta_y\right) = \left\{\int R_B\left[S E_s^{\downarrow} f\, \tau_1\tau_2 \cos\alpha + \varepsilon L_T\, \tau_2 + \tau_2 \int L_S\left(\theta,\phi\right)\cos\theta f\, d\Omega + L_u\right] d\lambda\right\} / \int R_B d\lambda \qquad (1)$$

where: all the radiometric terms are a function of wavelength

R_B is the relative spectral response (RSR) of band B,

S is the transmission through any objects along the sun-target path (ray tracer),

E_s^{ϕ} is the exo-atmospheric irradiance (MODTRAN) $\left[\mathrm{Wm^{-2}\mu m^{-1}}\right]$,

f is the target BRDF (ray tracer-texture map) $\left[\mathrm{sr^{-1}}\right]$,

τ_1 is the sun-target atmospheric transmission (ray tracer-MODTRAN),

τ_2 is the target-sensor atmospheric transmission (ray tracer-MODTRAN),

α is the angle from the normal to the target to the sun (ray tracer),

ε is the target emissivity (ray tracer-texture map),

L_T is the blackbody radiance from a target at target temperature T, (thermal model-ray tracer) $\left[\mathrm{Wm^{-2}sr^{-1}\mu m^{-1}}\right]$

L_S is the radiance from the θ,ϕ direction in the hemisphere above the target (it is calculated using MODTRAN if the background is sky and using a repeat of the target radiance calculations (i.e., Equation 1) if the background is not the sky) $\left[\mathrm{Wm^{-2}sr^{-1}\mu m^{-1}}\right]$,

$d\Omega$ is the element of solid angle in hemisphere above the target [sr],

L_u is the radiance due to scattering and self emission, along the target-sensor path (ray tracer-MODTRAN) $\left[\mathrm{Wm^{-2}sr^{-1}\mu m^{-1}}\right]$ and

$d\lambda$ is the element of wavelength $\left[\mu\mathrm{m}\right]$.

Note that all the MODTRAN terms are calculated for a specific user defined location, time of day, atmospheric profile and are a function of elevation, sensor zenith angle, and sensor azimuthal angle. In practice, the integrals in Equation 1 are solved using numerical approximations. The ray tracer is used to gather data $\left(L_S\right)$ from the hemisphere above the target in a user defined number of $\left(\theta,\phi\right)$ directions (typically about 100) and tens of spectral samples are used per spectral band.

The radiance given by Equation 1 is the effective spectral radiance that would be observed if we could sample the world with a delta function. In reality, we observe a blurred version of that value consisting of a weighted average of the radiance from the center of a pixel and its surround. This is obtained in DIRSIG by a numerical convolution of the $L_B\left(\theta_x,\theta_y\right)$ values with the sampled PSF of the instrument according to:

$$\hat{L}_B\left(\theta_x,\theta_y\right) = L_B\left(\theta_{\Delta x},\theta_{\Delta y}\right) * \mathrm{PSF}_B\left(\theta_{\Delta x},\theta_{\Delta y}\right) \qquad (2)$$

where $\hat{L}_B\left(\theta_x,\theta_y\right)$ is the effective radiance observed in band B for a detector centered on $\left(\theta_x,\theta_y\right)$, $L_B\left(\theta_{\Delta x},\theta_{\Delta y}\right)$ are the spectral radiance values from Equation 1 for a user defined number of samples across the PSF of the instrument, $*$ designates the discrete convolution function, and $\mathrm{PSF}_B\left(\theta_{\Delta x},\theta_{\Delta y}\right)$ is the discrete representation of the PSF in band B sampled on user defined steps of $\theta_{\Delta x},\theta_{\Delta y}$ about the nominal pixel center (see Figure 4). Note that in the first LDCM spiral, the PSF will only vary by band, however, as more test data becomes available the PSF can be varied by focal plane array or even by detector element.

Because the OLI and TIRS spectral detectors are not inherently registered, this process of sampling where each detector element is pointing and calculating the effective in band radiance must be repeated for each detector element (for each sample clock cycle). Conceptually, the sensor advances in its orbit between clock cycles and its external pointing geometry is updated as described in Section 2. After each clock cycle all the radiance values for all the detector elements sampled during that clock cycle are read out to a file. In addition, DIRSIG can write out a host of additional information for each detector element to support image assessment and algorithm development studies. These "truth" images can include scene data (X,Y,Z, class, temperature, sky fraction) and sensor data (noise, bias, gain…) that can be invaluable in trying to replicate and then debug and correct artifacts that occur in actual sensor data.

Initial Results

Because the focus of the first spiral was to simulate band-to-band misregistration effects in the OLI instrument, many aspects of the scene and sensor models were not implemented to expedite an early first release. Thus, all the results shown here are for OLI and do not include any jitter, noise or array-to-array or detector-to-detector variability. Figure 9a shows DIRSIG simulated images of OLI Blue and SWIR for portions of two focal plane arrays flown over a simplified version of the test scene. Floating Snellen Charts were included for debugging purposes. The images are shown as they would be clocked out (i.e., the vertical axis is common sample time for all images). Note that the odd-even detector offsets have been removed for display purposes, array-to-array offsets, band orientation reversal array-to-array and band-to-band offsets are all properly simulated in the DIRSIG images. The images are "unscrambled" in Figure 9b to account for the nominal odd-even, array-to-array and band-to-band pixel offsets. Figure 9c shows the orientation and approximate coverage of focal plane modules 07 and 08 over the DIRSIG scene explaining the various offsets and reversals in the image formation process. However, as illustrated in Figure 10 these nominal offsets will be insufficient to deal with proper band-to-band registration issues. In practice, the elevation of each pixel must be taken into account in calculating the proper amount to shift a pixel from one band to register it to another and to align the same band across arrays. Note that the actual shift required to align one pixel to another is a function of both local elevation variation, the effective height above the Geoid, and spacecraft altitude and thus will vary greatly around the globe. Thus, the USGS data processing of LDCM data will have to account for all the geometric and sampling effects. The DIRSIG data, by providing both "raw" imagery and "truth" from the "truth" images, can be used to support algorithm development and testing.

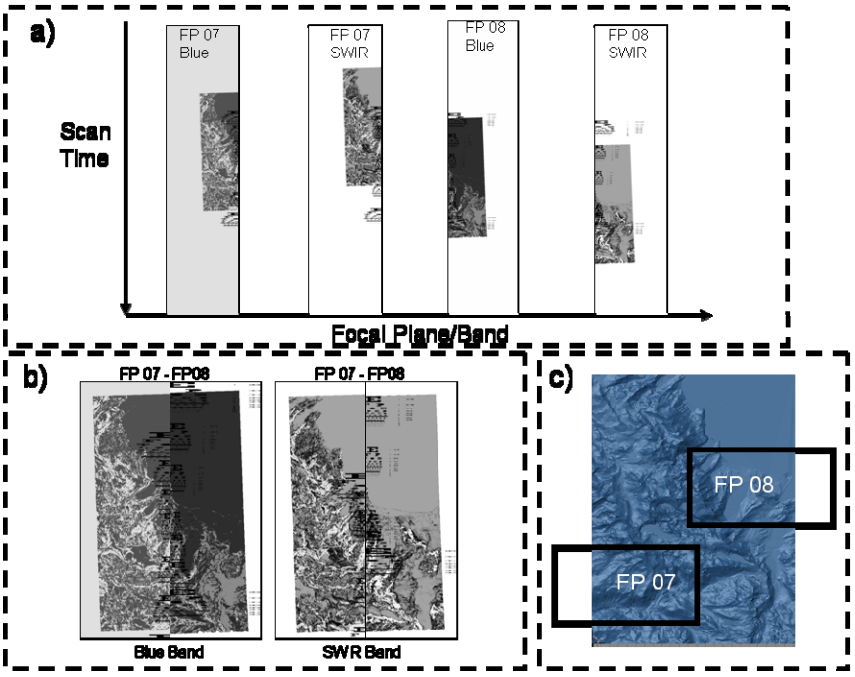

Figure 9. Preliminary image results for LANDSAT OLI DIRSIG simulation for the blue and SWIR bands of focal plane modules 7 and 8 flown over the test scene. **a)** Image order showing the readout including timing offsets between bands and modules (*N.B.*spectral bands have been offset for viewing). **b)** Images nominally aligned to remote timing offset. **c)** Approximate OLI focal plane 07 and 08 over DIRSIG test scene.

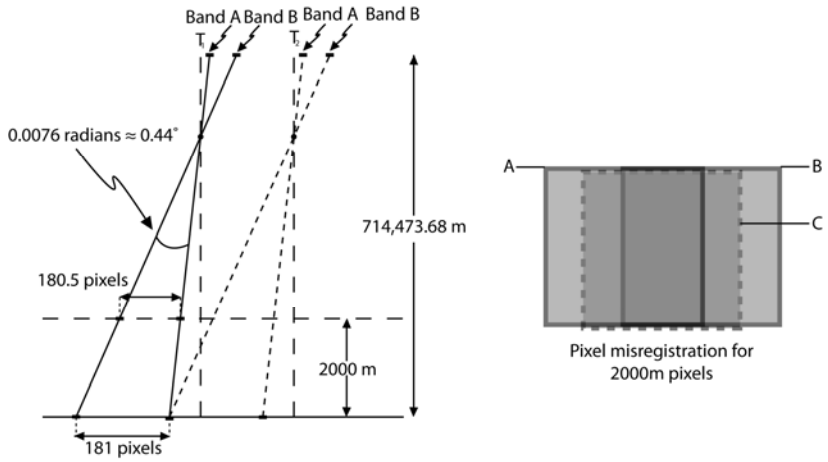

Figure 10. Illustration of how parallax effects in a push broom scanner cause pixels to be shifted by different amounts depending on elevation to achieve band-to-band registration.

Future Plans

The goal of the DIRSIG-LDCM effort is to provide ever increasing fidelity between the DIRSIG simulation and actual data from the LDCM sensors. This requires a number of improvements to the existing scene and sensor models. Many of the improvements are simply a matter of implementing existing DIRSIG capabilities using LDCM instrument specifications as they become available (e.g. array dependent RSRs, random noise levels…). Other capabilities will require modifications or enhancements to DIRSIG (e.g. control of array readout sequencing to generate a data stream that mimics LDCM, incorporating detector specific phenomenology like gain and bias variability, correlated noise…). As more and more functionality becomes available at each spiral, we expect DIRSIG to be a powerful tool in instrument development, algorithm development and test, on orbit initialization and evaluation of operational performance and anomaly assessment. Furthermore, to support the Landsat science community, scene physics and phenomenology will need to be expanded to support development and testing of applications algorithms. Short term goals for the next spiral are focused on an initial implementation of a TIRS instrument model and inclusion of the appropriate physics (thermal phenomena) in the Lake Tahoe test scene. As with the initial OLI implementation, the focus will be geometric phenomenology.

The list of longer term goals is quite extensive and the priority will be adjusted to meet program needs and speed of implementation. A number of known updates are associated with the detector modeling. These include RSRs, random and coherent noise, bias and gain variability, non linear response functions, structuring of readout streams and quantization settings. A similar set of updates are associated with the modeling of instrument PSF. These include modular PSF, incorporation of instrument motion on PSF (both in track and jitter, if warranted) and incorporation of detector specific capacitance effects on the PSF. Similarly, a number of improvements in the scene model have been identified to support both geometric and radiometric modeling. These include improving the reflectance spectral libraries by using an improved atmospheric compensation algorithm, adding BRDF models to the terrain, adding clouds to the scene and "planting" objects in the scene to further improve BRDF effects. The addition of texture maps to modulate bulk thermal properties is being considered to enhance the fidelity of TIRS simulations. Additional scenes and enlargement of the initial scene are also under consideration to support specific algorithm development and testing priorities. For example, maintaining co-registration of the OLI and TIRS instruments poses problems unique to the LDCM design. Selection and testing of appropriate scenes that will have high correlation across the thermal and reflective spectral bands takes on particular importance. DIRSIG may be able to help determine when particular targets would or would not be useful.

ACKNOWLEDGEMENTS

This material is based on work supported by NASA under award number NMX09AQ57A

REFERENCES

Hulley, G. C., S. J. Hook and A. M. Baldridge, 2008. ASTER Land Surface Emissivity Database of California and Nevada, *Geophysical Research Letters*, Vol. 35.

Irons, J.R., Murphy-Morris, J., 2007. Geoscience and Remote Sensing Symposium, 2007. IGARSS 2007. IEEE International 23-28 July 2007 Page(s):2808 - 2810 Digital Object Identifier 10.1109/IGARSS.2007.4423426.

Markham, Brian L., Philip W. Dabney, James C. Storey, Ron Morfitt, Edward J. Knight, Geir Kvaran and Kenton Lee, 2008. Landsat Data Continuity Mission Calibration And Validation, ASPRS 2008, Pecora 17: The Future of Land Imaging . . . Going Operational, Denver, Co., November 2008.

Sanders, L.C., Schott, J.R., and Raqueño, R.V., 2001. A VNIR/SWIR atmospheric correction algorithm for hyperspectral imagery with adjacency effect, *Remote Sensing of Environment,* Vol. 77, p. 1-11.

Scanlan, N.W., Schott, J.R. Brown, S.D., 2003. Performance analysis of improved methodology for incorporation of spatial/spectral variability in synthetic hyperspectral imagery**,** Proceedings of SPIE, Vol. 5159, pp 319-330, San Diego, August 2003.

Schott J.R., R. Raqueño, C. Salvaggio, 1992. Incorporation of a time-dependent thermodynamic model and a radiation propagation model into infrared 3-D synthetic image generation, *Journal of Optical Engineering*, Vol. 31 #7 pp. 1505-1516, July 1992.

Schott, J.R., Brown, S.D., Raqueño, R.V., Gross, H.N., & Robinson, G. 1999. An advanced synthetic image generation model and its application to multi/hyperspectral algorithm development, *Canadian Journal of Remote Sensing*, Vol. 25, No.2, pp. 99-111, June 1999.

Schott, J.R., 2007, *Remote Sensing: The Image Chain Approach, 2nd Ed*., Oxford University Press.

Vallado, David A. and Paul Crawford, 2008, SGP4 Orbit Determination, AIAA/AAS Astrodynamics Specialist Conference and Exhibit, AIAA 2008-6770, Honolulu, Hawaii, August 2008.

Ward, J.T., J.R. Schott, N.J. Sanders, S.D. Brown, 2008. Driving Realistic Texture in Simulated Long Wave Infrared Imagery, *Proceedings of IGARSS*, Vol. 3, pp. 728-731, Boston, July 2008.